ACS APPLIED MATERIALS & INTERFACES

Research Article

www.acsami.org

Heparin-Mimicking Multilayer Coating on Polymeric Membrane via LbL Assembly of Cyclodextrin-Based Supramolecules

Jie Deng,[†] Xinyue Liu,[†] Lang Ma,[†] Chong Cheng,*[,†,‡] Wenbin Shi,[†] Chuanxiong Nie,[†] and Changsheng Zhao*[,†,§]

[†]College of Polymer Science and Engineering, State Key Laboratory of Polymer Materials Engineering, Sichuan University, Chengdu 610065, China

[‡]Department of Chemical Engineering, Department of Biomedical Engineering, University of Michigan, Ann Arbor, Michigan 48109, United States

[§]National Engineering Research Center for Biomaterials, Sichuan University, Chengdu 610064, China

Supporting Information

ABSTRACT: In this study, multifunctional and heparin-mimicking star-shaped supramolecules-deposited 3D porous multilayer films with improved biocompatibility were fabricated via a layer-by-layer (LbL) self-assembly method on polymeric membrane substrates. Star-shaped heparin-mimicking polyanions (including poly(styrenesulfonate-*co*-sodium acrylate; Star-PSS-AANa) and poly(styrenesulfonate-*co*-poly(ethylene glycol)methyl ether methacrylate; Star-PSS-EGMA)) and polycations (poly(methyl chloride-quaternized 2-(dimethylamino)ethyl methacrylate; Star-PMeDMA) were first synthesized by atom transfer radical polymerization (ATRP) from *β*-cyclodextrin (*β*-CD) based cores. Then assembly of 3D porous multilayers onto polymeric membrane surfaces was carried out by alternating deposition of the polyanions and polycations via electrostatic interaction. The surface morphology and composition, water contact angle, blood activation, and thrombotic potential as well as cell viability for the coated heparin-mimicking films were systematically investigated. The results of surface ATR-FTIR spectra and XPS spectra verified successful deposition of the star-shaped supramolecules onto the biomedical membrane surfaces; scanning electron microscopy (SEM) and atomic force microscopy (AFM) observations revealed that the modified substrate had 3D porous surface morphology, which might have a great biological influence on the biointerface. Furthermore, systematic in vitro investigation of protein adsorption, platelet adhesion, human platelet factor 4 (PF4, indicates platelet activation), activate partial thromboplastin time (APTT), thrombin time (TT), coagulation activation (thrombin-antithrombin III complex (TAT, indicates blood coagulant)), and blood-related complement activation (C3a and C5a, indicates inflammation potential) confirmed that the heparin-mimicking multilayer coated membranes exhibited ultralow blood component activations and excellent hemocompatibility. Meanwhile, after surface coating, endothelial cell viability was also promoted, which indicated that the heparin-mimicking multilayer coating might extend the application fields of polymeric membranes in biomedical fields.

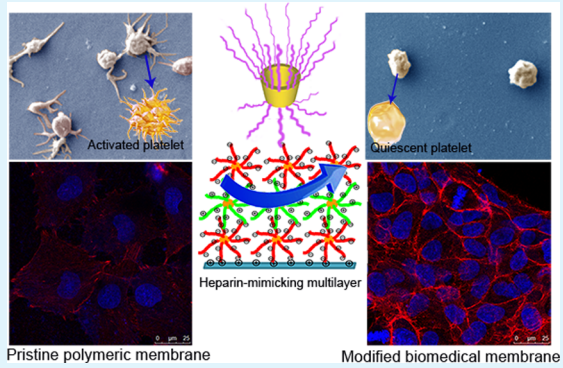

KEYWORDS: *β-cyclodextrin, star-shaped supramolecules, layer-by-layer assembly, heparin-mimicking multilayer, blood and cell compatibility, polymeric membranes*

1. INTRODUCTION

Synthesis of novel, low-cost, effective antithrombogenic biomacromolecules and their applications in biointerface modification have been of great interest in the fields of blood-contacting biomaterials, such as disposable blood collecting devices, clinical hemodialysis membrane, cardiopulmonary bypass device, and replacement implants as well as the newly developed hemocompatible drug or antibody nanocarriers.[1] When the foreign materials contact with blood, plasma protein adsorption is the first step of bioresponses between the blood and the materials followed with the adhesion or activation of clotting enzyme and platelets[2] and sequentially leads to formation of a nonsoluble fibrin network or thrombus. A recent investigation indicated that heparin and heparin-mimicking polymers could be used to modify the blood-contacting biomaterials.[3] Different from many traditional antifouling or hemocompatible surface designs,[4] a large amount of research indicated that the heparin and heparin-mimicking polymer-immobilized surfaces exhibited integrated remarkable anticoagulant bioactivity, diminished thrombogenic response,

Received: September 26, 2014
Accepted: November 6, 2014
Published: November 6, 2014

and cell attachment ability.[5] Moreover, the heparin and heparin-like polymers showed significant promotion on the angiogenesis while reducing the need for exogenous growth factors during in vivo studies.[6] However, being an animal-derived product, utilization of heparin in surface systems might have potential side effects;[7] furthermore, the high cost for producing heparin also inhibits its use in large-scale biomaterial surface modification. Modification or development of advanced biomaterials by mimicking the structure and function of biomacromolecules has long been an ideal goal in various modification approaches.[8−10] In our recent studies, great efforts have been made to design heparin-mimicking polymers to endow the modified blood-contacting materials with heparin-mimicking biological ability.[3,5,11] The designed heparin-mimicking interfaces have excellent antithrombogenic ability and improved blood and cell compatibility, which may have a large impact on advancement of blood-compatible biomaterials.

To date, considerable methods have been utilized to functionalize the membranes with a heparin-mimicking surface, such as bulk blending, plasmas treatment, grafting, coating, or layer-by-layer (LbL) assembly, etc.[3,12−16] Meanwhile, these studies have confirmed that the heparin-mimicking methods could improve blood compatibility and extend potential applications of the biomedical materials. However, to design the next generation multifunctional biomedical membranes, the heparin-like linear polymers are insufficient to meet the challenges required for multifunctionality with tunable surface morphologies along with extended biological activity. For the heparin-like linear polymer-assembled surfaces, 2D dense layers were usually obtained as a well-established assembly of polyelectrolytes. Compared to linear polymers, star-shaped supramolecules consist of large numbers of linear arms connected to the central core, which would increase the densities of the bioactive or functional groups. Among the newly emerged methods, research on surface-engineered self-assembly of functional multilayers has attracted interest in various biomedical applications, such as drug encapsulation and sustained release, cell and tissue scaffolds, stem cell differentiation, as well as artificial organs and devices.[17−20] The surface self-assembly strategy is regarded as one of the most promising approaches to obtain a tunable coating morphology and endow the biointerface with excellent blood and cell compatibility. Various new functional building blocks ranging from nanoparticles, nanotubes, nanosheets, and nano/microgels have been extensively exploited and applied to construct multilayer thin films,[21−23] and the modified biomaterials exhibit versatile biological functions and activities. Furthermore, the nanomaterials-assembled multilayers could overcome the inherent drawbacks of polyelectrolytes-assembled dense 2D layers, which can endow the biointerface with porous structure and a high density of bioactive or functional groups/molecules. Thus, the heparin-like polymers-integrated nanomaterials could endow great benefits for modification of blood-contacting materials. However, the procedure for preparation of these nanomaterials is usually complicated and expensive. Thus, a highly synthetic and low-cost approach should be developed, which would greatly advance construction of multifunctional biomedical membranes.

Recently, cyclodextrin (CD) molecules have been used to construct hyperbranched polymers for various functional applications.[24,25] The 3D structure of the CD molecule can be considered as a truncated cone, which has 21 hydroxyl groups located at the fringe of CD. Numerous functional groups can be introduced onto CD via esterification between the functional molecules and the hydroxyl groups on CD. Li et al. reported a CD-based star-shaped hyperbranched water-soluble cationic polymer via atom transfer radical polymerization (ATRP).[26] Xu et al. prepared a CD-based star-shaped cationic supramolecule via ATRP for gene delivery, and the CD core can improve the gene transfection efficiency.[27] Furthermore, the CD-based star-shaped hyperbranched polymers can also assemble into diverse morphologies with 3D architectures in aqueous solution by controlling the macromolecular architecture and the compositions of the polymers.[28] Inspired by the star-shaped hyperbranched structure, the CD-based star-shaped supramolecules might be used as building blocks in surface construction of a 3D porous multilayer thin film for modification of biomedical membranes.

Herein, in the present study, promoted by the synthesis of inexpensive and commonly available CD core-based 3D star-shaped supramolecules, biocompatible 3D porous multilayers are prepared via the LbL assembly of CD-based polyanions and polycations alternately. Polycations (Star-PMeDMA) and polyanions (Star-PSS-AANa and Star-PSS-EGMA) were synthesized via ATRP from CD-based cores. A general concept of heparin-mimicking polymers can be defined as the heparin sulfates or synthetic sulfated/carboxylated polymers with comparable biologically mimicking functionalities as heparin. Thus, the sulfonic acid, carboxyl acid groups, and ether linkages in Star-PSS-AANa and Star-PSS-EGMA gave the possibility to synthesize new-fashioned hyperbranched heparin-mimicking biomacromolecules. The star-shaped supramolecules were then allowed for LbL assembly on a poly(ethylene imine) (PEI) precoated membrane substrate; the ionic interaction between the polycations and polyanions led to the deposition to form surface 3D porous thin films. ATR-FTIR, XPS, and scanning electron microscopy (SEM) were applied to confirm the chemical components and interface-assembled 3D porous architecture. Meanwhile, the blood activation and compatibility of the supramolecules-assembled membranes were explored in detail by wettability, plasma protein adsorption, platelet adhesion, human platelet factor 4 (PF4, indicates platelet activation), activated partial thromboplastin time (APTT), thrombin time (TT), coagulation activation (thrombin-antithrombin III complex (TAT, indicates blood coagulant)), and blood-related complement activation (C3a and C5a, indicates inflammation potential). Meanwhile, cell viability was confirmed using endothelial cells.

2. EXPERIMENTAL SECTION

2.1. Materials. Cyclic ligand 5,7,7,12,14,14-hexamethyl-1,4,8,11-tetra-azacyclo-tetradecane (Me_6TATD) was synthesized according to the literature.[29] β-Cyclodextrin (β-CD, 98%, Aladdin) was dried over $CaCl_2$ at 80 °C under vacuum for 24 h before use. Bromoisobutyryl bromide (BIBB, 98%), poly(ethylene glycol) methyl ether methacrylate (PEGMA), *N*,*N*,*N*′,*N*″,*N*″-pentamethyldiethylenetriamine (PMDETA, 99%), sodium 4-vinylbenzenesulfonate (SSNa, 90%), [2-(methacryloyloxy)ethyl]trimethylammonium chloride solution (75 wt % in water), and sodium acrylate (AANa) were purchased from Aladdin Reagent Co. Ltd. (China). More detailed information for materials was included in the Supporting Information.

2.2. Synthesis of $(Br)_{19}$-β-CD Macroinitiator. The procedure for synthesis of macroinitiator was according to the literature.[30,31] β-CD (1.7 g, 1.5 mmol) and triethylamine (3.5 g, 34.56 mmol) were dissolved in 15 mL of anhydrous 1-methyl-2- pyrolidinone (NMP) under stirring, and then the flask was immersed into an ice−water bath. BIBB (7.954 g, 34.56 mmol) dissolved in 8 mL of anhydrous

Scheme 1. Synthesis Route of CD-Based Macroinitiator and Polymerization of Star-Shaped Supramolecules via ATRP (A); Procedures for Preparation of LbL Assembly of 3D Porous Multilayer Thin Films on Membrane Substrates (n = 4, 14, 24 (B))

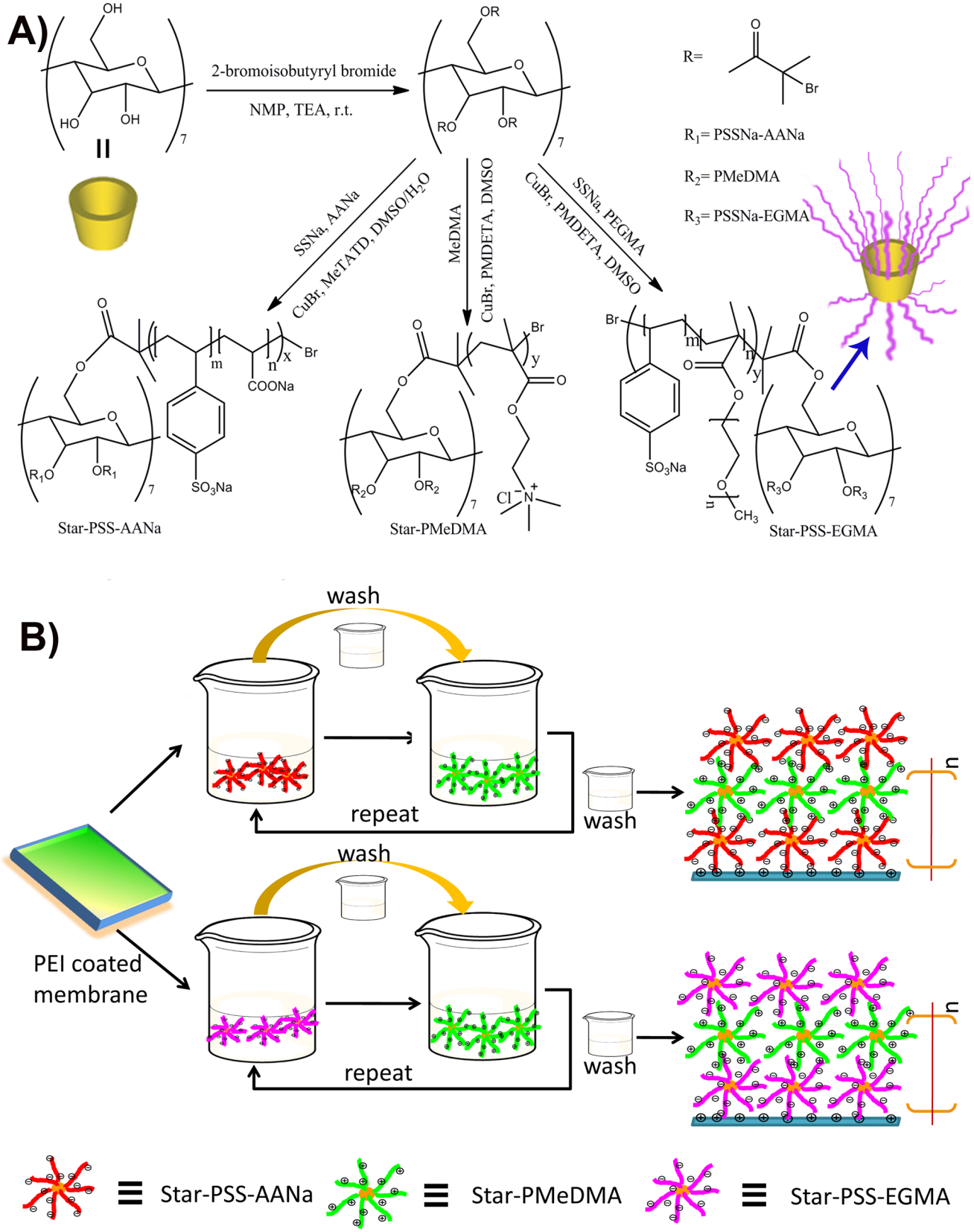

NMP was then added dropwise into the β-CD solution. The reaction temperature was maintained at 0 °C for 2 h and then for another 24 h at room temperature; then the white solid was filtered off. The filtrate was purified with dialysis membrane (MWCO = 1000) against DI water for 3 days, followed by freeze drying to give the macroinitiator (Scheme 1A). The obtained β-CD-Br macroinitiator exhibited 19

dx.doi.org/10.1021/am506249r | ACS Appl. Mater. Interfaces 2014, 6, 21603−21614

grafted sites and was named $(Br)_{19}$-β-CD, which will be discussed in the Results and Discussion section.

2.3. Polymerization of Star-Shaped Supramolecules. *2.3.1. Synthesis of Star-Shaped Heparin-Mimicking Anionic Polymers (Star-PSS-AANa and Star-PSS-EGMA) via ATRP.* Star-PSS-AANa was synthesized by ATRP using $(Br)_{19}$-β-CD as the macroinitiator and SSNa and AANa as monomers. Typically, $(Br)_{19}$-β-CD (0.2 g, 0.05 mmol), SSNa (8.005 g, 38.8 mmol), AANa (2.376 g, 25.3 mmol), and 22 mL of mixed solvent of dimethyl sulfoxide (DMSO) and DI water (v/v 8/14 mL) were added to a Schlenk tube, followed by addition of Me_6TATD (0.34 g, 1.2 mmol) and CuBr (0.136 g, 0.95 mmol) under a N_2 atmosphere. Then the tube was closed by a three-way stopcock. After three freeze−pump−thaw cycles the tube was sealed off in a N_2 atmosphere. The reaction was carried out at 70 °C for 24 h and subsequently exposed into air to terminate polymerization. Afterward the reactant mixture was purified with dialysis membrane (MWCO 8000−14 000) against NaCl solution and ethanol alternatively for 1 week, and then the resulted solution was freeze dried to obtain star-shaped supramolecules. The synthesis procedure of Star-PSS-EGMA was similar to that of Star-PSS-AA. Briefly, $(Br)_{19}$-β-CD (0.1 g, 0.025 mmol), SSNa (1.946 g, 9.43 mmol), and PEGMA (2.989 g, 6.3 mmol) were added to a Schlenk tube containing 20 mL of DMSO, followed by addition of PMDETA (0.171 g, 0.88 mmol) and CuBr (0.068 g, 0.475 mmol) under a N_2 atmosphere. Then the tube was closed by a three-way stopcock. After three freeze−pump−thaw cycles, the tube was sealed off in a N_2 atmosphere. The reaction was carried out at 70 °C for 24 h and subsequently exposed into air to terminate polymerization. The subsequent purification procedure was the same as Star-PSS-AANa.

2.3.2. Synthesis of Star-Shaped Cationic Polymer (Star-PMeDMA) via ATRP. $(Br)_{19}$-β-CD (0.2 g, 0.05 mmol), MeDMA (9.89 g, 47.6 mmol), and DMSO (30 mL) were added to a Schlenk tube, followed by addition of PMDETA (0.342 g, 1.76 mmol) and CuBr (0.136 g, 0.95 mmol) under a N_2 atmosphere. Then the tube was closed by a three-way stopcock. After three freeze−pump−thaw cycles the tube was sealed off in a N_2 atmosphere. The reaction was carried out at 70 °C for 24 h and subsequently exposed to air to terminate polymerization. Afterward the reactant mixture was purified with dialysis membrane (MWCO 8000−14 000) against DI water for 3 days followed by freeze drying to obtain star-shaped supramolecules.

2.4. Preparation of PEI-Coated Polymeric Membranes. Typically, poly(ether sulfone) (PES) membranes were selected as model substrates, which were prepared using a phase transition method as described in our previous report.[32] The homemade PES membrane was cut into pieces with an area of 1 × 1 cm^2, which was then immersed into a PEI aqueous solution (20 mg/mL) and shaken at 37 °C for 6 h. Afterward, the membranes were rinsed with a large amount DI water and then dried under vacuum at 40 °C overnight to obtain PEI-coated PES membranes.[14,33]

2.5. Layer-by-Layer Self-Assembly of Star-Shaped Supramolecules on Polymeric Membrane Surface. Using the heparin-mimicking and polycation star-shaped supramolecules, the surface LBL assembly process was carried out on a typical polymeric membrane, PES membrane, which had been widely used in hemodialysis, artificial organs, filtration, water treatments, etc. Aqueous solutions of Star-PSS-AANa (5 mg/mL), Star-PSS-EGMA (5 mg/mL), and Star-PMeDMA (5 mg/mL) were prepared prior to use. Multilayer growth was performed manually. The substrates of PEI-coated PES membranes were dipped into the Star-PSS-AANa (or Star-PSS-EGMA) solution for a period of 15 min and subsequently rinsed with DI water. The membranes were then transferred to the Star-PMeDMA solution for a period of 15 min, after which they were rinsed and the process was repeated (Scheme1B).[34] Membranes with 5, 15, and 25 bilayers were obtained by alternating sequential deposition in polyanion and polycation solutions. The membranes deposited with Star-PSS-AANa and Star-PMeDMA were obtained as M-SA, while the membranes assembled with PSS-EGMA and Star-PMeDMA were obtained as M-SE. All the prepared bilayer membranes exhibited with the polyanion as the outermost layer. Furthermore, the surface coatings of polyvinylidene difluoride (PVDF) and polysulfone (PSf) membranes with 15 bilayers were conducted using a similar process as PES membranes.

2.6. Characterization. ^{1}H NMR spectra were obtained via a Bruker spectrometer (400 MHz).A FTIR spectrometer (Nicolet 560, USA) and X-ray photoelectron spectrometer (XSAM800, Kratos Analytical, UK) were used to detect the surface composition of the membranes. The nanosizes and zeta potentials in aqueous solutions for the three kinds of star-shaped supramolecules were performed via dynamic light scattering (DLS, Zetasizer ZS90, Malvern Instruments). Field emission scanning electron microscope (FE-SEM) images were acquired using a scanning electron microscope (JSM-7500F, JEOL, Japan). AFM images of the modified membranes were obtained using a Multimode Nanoscope V scanning probe microscopy (SPM) system (Bruker, USA).

The interface hydrophilicity of the modified membranes was investigated via water contact angle using a contact angel goniometer (OCA20, Dataphysics, Germany, equipped with a video capture). The measurement error was ±3°.

2.7. Blood Compatibility. *2.7.1. Protein Adsorption.* Evaluation of protein adsorption was performed according to our previous report.[14] Briefly, the as-prepared membranes (1 × 1 cm^2) were first immersed in normal saline overnight at 4 °C, followed by incubating at 37 °C for 1 h. Afterward, the membranes were immersed in a phosphate buffer solution (PBS) containing bovine serum albumin (BSA) (or bovine serum fibrinogen (FBG)) with a concentration of 1 mg/mL. The membranes were subsequently rinsed cautiously with PBS solution and double-distilled water after being incubated at 37 °C for another 1 h.

2.7.2. Platelet Adhesion. To avoid the interference of other components (such as leucocyte and erythrocyte) in the blood, platelet-rich plasma (PRP) was utilized to study platelet adhesion for the pristine PES surface and star-shaped polymers-deposited 3D multilayer thin films. Healthy human fresh blood (man, 28 years old) was collected by vacuum tubes, containing sodium citrate as the anticoagulant (blood to anticoagulant ratio, 9:1 v/v), which was then centrifuged at 1000 rpm for 15 min to obtain PRP.[35] Detailed procedures for platelet adhesion experiments were described in the Supporting Information.

2.7.3. Clotting Time. In the clinical application, APTT and TT measurements were widely used to detect the abnormality of blood plasma and primarily check the anticoagulative chemicals, while recently they were applied to evaluate the in vitro antithrombogenicity of blood-contacting biomedical materials.[36] Generally, APTT was used to detect the efficacy of both the common coagulation pathways and the intrinsic pathway including fibrinogen, prothrombin, and blood coagulation factor V, X in plasma in an endogenous pathway of coagulation. TT was applied to test the time taken for formation of a clot in the plasma in which an excess of thrombin had been supplied.[37] Thus, in this study, to further evaluate the anticlotting and antithrombotic ability of the heparin-mimicking layer, platelet-poor plasma (PPP) was utilized to measure the APTT and TT via an automated blood coagulation analyzer CA-50 (Sysmex Corp., Kobe, Japan). Procedures were described in our previous reports in detail.[38]

2.7.4. Contact Activation of Coagulation System (platelet activation and thrombin generation). Platelet activation (PF4) and coagulation activation (TAT) were evaluated via commercial enzyme-linked immunosorbent assays (ELISA). Whole blood was incubated with the pristine and star-shaped polymers-coated samples for 2 h and centrifuged at 1000*g* (4 °C) centrifugal force for 15 min to obtain plasma. Then detections were conducted according to the respective instructions from the manufacturer.

2.7.5. Complement Activation in Human Blood System. The same as the PF-4 and TAT tests, the complement activation (C3a and C5a) evaluation for these samples was also carried out with the ELISA method (CUSABIO BIOTECH CO., LTD, China). Complement activation, generated by the localized inflammatory mediator, which is the trigger of the host defense mechanism, is another vital aspect of blood compatibility.[39] The whole blood incubated with the pristine and star-shaped polymers-coated samples for 2 h was centrifuged at 1000*g* (4 °C) centrifugal force for 15 min to obtain plasma. Then

detections were performed according to the respective instructions from the manufacturer.

2.8. Cytocompatibility. *2.8.1. Cell Culture.* Human umbilical vein endothelial cells (HUVECs) were cultured in R1640 medium containing supplements of 10% fetal bovine serum (FBS, Hyclone, America), 2 mM L-glutamine, and 1% (V/V) antibiotics mixture (10000 U of penicillin and 10 mg of streptomycin). Pristine PES membrane and star-shaped supramolecule-deposited membranes (1 × 1 cm^2) were first immersed into the cell culture medium for 3 h at 37 °C in a cell incubator. Afterward, membranes were transferred into 24-well cell-culture plates, rinsed with PBS, and sterilized by UV irradiation; then HUVECs with a density of approximately 2.5 × 10^4 cells/cm^2 were seeded onto the membranes.

2.8.2. Cell Morphology on the Membranes. For SEM observation, seeded membranes with 6 day culture were dried by passing through a series of graded alcohol–PBS solutions and then dehydrated through isoamyl acetate–alcohol solutions followed by the liquid CO_2 critical point drying.

2.8.3. 3-(4,5-Dimethylthiazol-2-yl)-2,5-diphenyltetrazolium Bromide (MTT) Assay. Viabilities of the HUVECs were evaluated via MTT assay after the cells were cultured for 2, 4, and 6 days. The optical density of the formazan solution was calculated by a Microplate reader (model 550, Bio-Rad) at 492 nm. To minimize the test error, eight samples for each type of membranes were measured. Results were expressed as means ± SD. The statistical significance was evaluated by the Student's *t* test, and the level of significance was chosen as $P < 0.05$.

2.8.4. Confocal Imaging. HUVECs grown under standard culture condition were seeded onto the PES and star-shaped polymer-deposited membrane surfaces at 2.5 × 10^4 cells/cm^2 and cultured for 6 days, at which time they were fixed with formaldehyde (3.7% in PBS) at 4 °C overnight and then stained with rhodamine-conjugated phallodin and 4′,6-diamidino-2-phenylindole (DAPI) according to the instruction manuals. Fluorescent images of the sample were obtained via confocal laser scanning microscopy (Leica, Switzerland).

3. RESULTS AND DISCUSSION

3.1. Characterization of the Macroinitiator. In brief, 2-bromoisobutyryl bromide was first grafted onto CD (Br-*β*-CD). Figure 1A shows the FTIR spectra for pure *β*-CD and Br-*β*-CD. The signals at 1156 and 3387 cm^{-1} in the spectrum of *β*-CD were assigned to deformation of O–C groups and the stretching vibration of hydroxyl groups (ν_{O-H}), respectively. The peaks at 1414 and 1334 cm^{-1} in the same spectrum were ascribed to deformation of O–H. The signal at 1739 cm^{-1} in the spectrum of Br–*β*-CD was assigned to the stretching vibration of carbonyl groups ($\nu_{C=O}$). The signals at 1462 and 1390 cm^{-1} were attributed to the asymmetric C–H and symmetric C–H bending of CH_3 groups, respectively. The band at 1271 cm^{-1} was ascribed to the asymmetric vibration of C—(C=O)—O, and the band at 650 cm^{-1} corresponded to the stretching vibration of the C–Br groups, which indicated formation of the Br–*β*-CD macroinitiator.[31] Then, as shown in Figure 1B and 1C, successful synthesis of the Br–*β*-CD macroinitiator was further confirmed by the ^{1}H NMR spectra. The characteristic signals of the synthesized Br–*β*-CD in this study appeared to be consistent with the earlier report.[31] Meanwhile, the number of grafted initiator groups per molecule of *β*-CD was 19 and calculated from the ^{1}H NMR spectra: *δ* 1.2–2.2 (114H, CH_3), 3.5–5.5 (51H, residues of *β*-CD); thus, the *β*-CD–Br macroinitiator was named $(Br)_{19}$–*β*-CD.

3.2. Synthesis and Characterization of the Star-Shaped Supramolecules. It has been reported that with a high local concentration of initiator sites of the $(Br)_{19}$–*β*-CD radical–radical coupling of the propagating chains would probably occur, resulting in gelation.[28] In this work, polymerization was carried out with different concentrations of macroinitiator and monomers. It was found that polymerization resulted in gelation with a high concentration of the macroinitiator or monomers, which also happened in some earlier reported procedures (data not shown). FTIR spectra were applied to confirm the chemical structures of these star-shaped supramolecules (Figure S1, Supporting Information); all chemical units were indicated by these characteristic peaks.

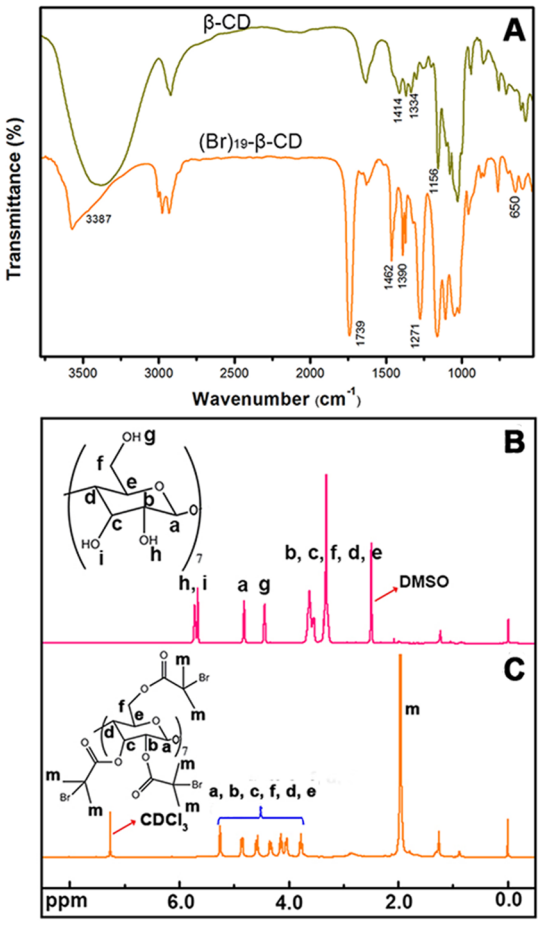

Figure 1. (A) FTIR spectra of *β*-CD and $(Br)_{19}$–*β*-CD. (B) ^{1}H NMR spectrum of *β*-CD in DMSO.(C) ^{1}H NMR spectrum of $(Br)_{19}$–*β*-CD in $CDCl_3$.

Furthermore, Table 1 shows the average diameters and zeta potentials for the star-shaped supramolecules after dissolving in DI water (note, all of the synthesized star-shaped supramolecules could be easily dissolved in water with no pH control or buffer). As shown in Table 1, the synthesized star-shaped supramolecules possessed an average diameter of about 100–150 nm in DI water. The zeta potentials for Star-PMeDMA,

Table 1. Diameters and Zeta Potentials for Star-PMeDMA, Star-PSS-AANa, and Star-PSS-EGMA (in DI water)[a]

star-shaped supramolecules	diameter in DI water (nm)	zeta potential in DI water (mV)
Star-PMeDMA	104.5 ± 25.2	+19.6 ± 1.2
Star-PSS-AANa	123.1 ± 20.0	−38.6 ± 2.7
Star-PSS-EGMA	140.2 ± 23.4	−33.4 ± 1.6

[a]Data are presented as the average values of triplicate measurements with standard deviations. Sample concentration 0.1 mg/mL.

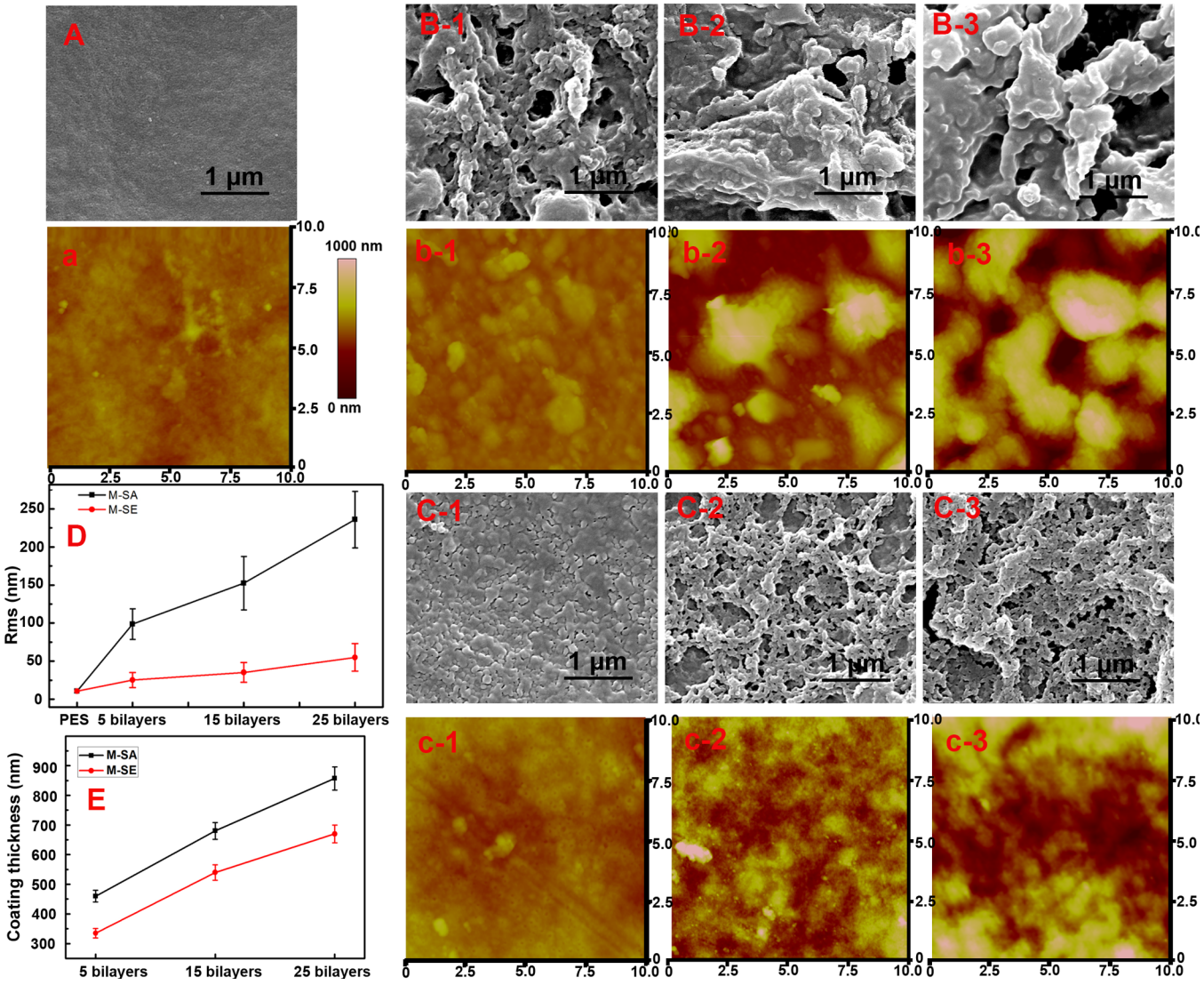

Figure 2. Typical SEM images of the surface morphologies for pristine PES membrane (A), M-SA (B-1, M-SA-5; B-2, M-SA-15; and B-3, M-SA-25), and M-SE (C-1, M-SE-5; C-2, M-SE-25; and C-3, M-SE-25). AFM images of the membranes for pristine PES membrane (a), M-SA (b-1, M-SA-5; b-2, M-SA-15; and b-3, M-SA-25), and M-SE (c-1, M-SE-5; c-2, M-SE-25; and c-3, M-SE-25). Surface roughness calculated from 5 AFM images (D). Coating thickness measured from 5 cross-section SEM observation (E); cross-section SEM images of M-SA-15 and M-SE-15 are shown in Figure S7, Supporting Information.

Star-PSS-AANa, and Star-PSS-EGMA were +19.6, −38.6, and −33.4 mV, respectively. It could be observed that Star-PSS-AANa was more negative compared to Star-PSS-EGMA, which result from the existence of the neutral EGMA fragments in Star-PSS-EGMA.

3.3. Membrane Characterization. *3.3.1. Surface Morphology of the 3D Porous Layer.* Typical SEM observations for the pristine membrane surface and star-shaped supramolecule-deposited 3D porous thin film surfaces are shown in Figure 2 (A, B-1, B-2, B-3, C-1, C-2, and C-3). It was noticed that the pristine membrane had an even surface morphology, while obviously the star-shaped supramolecule-assembled substrates exhibited 3D porous surface structures, especially the M-SA membranes. An interesting phenomenon was observed that there was a large difference in the surface morphology between the M-SA and the M-SE. The M-SA membranes were much rougher than the membranes of M-SE. Furthermore, with the increase of the bilayers from 5 to 25, the surface roughness of M-SE increased gradually and the M-SE membranes showed more homogeneous surface 3D structures than M-SA. The star-shaped supramolecule-assembled PVDF and PSf membrane surfaces with 15 bilayers were also examined by SEM images (Figure S2, Supporting Information); the coating surface also exhibited 3D porous morphologies as PES membrane surface, which indicated that this proposed strategy could also be applied in the surface coating of many other polymeric membrane substrates.

AFM (with a tapping mode at a scan rate of 0.8 Hz over an area of 10 × 10 μm^2) was further used to evaluate the surface morphology and roughness of the star-shaped supramolecule-deposited multilayer surfaces. As shown in Figure 2 (a, b-1, b-2, b-3, c-1, c-2, and c-3), the surface of the pristine membrane was clearly verified to be a characteristic 2D flat surface, while after assembly of the star-shaped supramolecules 3D porous structures were observed on the membrane surfaces, which showed an identical result to the SEM observation. As shown in Figure 2D, Rms was used to evaluate the average surface roughness of these membranes. It was observed that the

surfaces of the M-SA membranes were much rougher than those of the M-SE membranes; the surface roughness of the M-SA membranes increased dramatically with the increase of the coating bilayers from 5 to 25. However, the M-SE membranes showed slightly increased surface roughness with the increase of the bilayers from 5 to 25. Though it was hard to detect the detailed assembly mechanism between these two star-shaped supramolecules, the different surface-assembled morphologies should be greatly influenced by the AA and EGMA segments. During assembly the EGMA fragments might twine around each other.[40] In addition, introduction of EGMA fragments decreased the negative charge of the Star-PSS-EGMA; thus, the repulsion between the Star-PSS-EGMA molecules was lower than that for Star-PSS-AANa, which might also lead to the lower roughness of M-SE. In general, after LbL coating of the star-shaped supramolecules both of the membranes showed 3D surface architectures compared to the pristine membrane.

3.3.2. ATR-FTIR and XPS Spectra of the Membrane Surfaces. Surface ATR-FTIR and XPS spectra confirmed that the star-shaped supramolecules were successfully deposited onto the polymeric membrane surfaces, as discussed in detail in the Supporting Information (Figure S3).

3.3.3. Water Contact Angle (WCA) Analysis. WCA measurement was utilized to estimate the wettability property of the as-prepared membranes. As shown in Figure 3B together

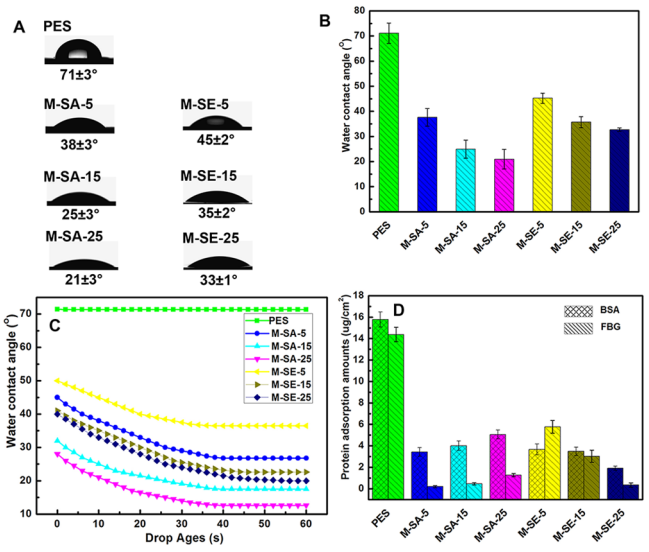

Figure 3. Representative pictures of water contact angles (taken at 10 s) from independent experiments are shown at left (A). Static water contact angles of pristine PES and star-shaped supramolecule-deposited membranes (B). Measurements of water contact angles with increased contacting time (C). Bovine serum albumin (BSA) and bovine serum fibrinogen (FBG) adsorption amounts onto the membranes (D); values are expressed as means ± SD, n = 3.

with the corresponding images taken from the membrane (Figure 3A), the contact angle of the pristine polymeric membrane was 71.1°, while the star-shaped supramolecule-deposited 3D porous surfaces possessed much lower WCAs. The WCAs for the star-shaped supramolecules-assembled surfaces notably decreased to ranging from 45° to 20°, and the modified surfaces became more hydrophilic with the increase of the bilayers. It was interesting to find that the M-SA had a much lower water contact angle than the M-SE, which might be due to the fact that the M-SA possessed a more porous surface morphology than the M-SE, while static water contact angle measurements alone were not adequate to evaluate hydrophilicity. To better evaluate the hydrophilicity of the porous multilayers, the changes of water contact angle with increased contacting time were also carried out, and the results indicated that the 3D porous multilayers revealed decreased water contact angle with increasing time, which further confirmed that the 3D porous multilayers-modified membranes become much more hydrophilic than the pristine polymeric membrane (Figure 3C).

3.4. Blood Compatibility. *3.4.1. Protein Adsorption.* The adsorbed protein amount on a material surface is reported to be one of the most important factors in evaluating the blood compatibility of biomedical material.[41] It is well known that a material with a more hydrophilic surface generally shows a lower amount of protein adsorption.[42] In this study, both of the BSA and BFG adsorptions were measured, and the results are shown in Figure 3D. It could be noticed that the membranes of M-SA showed a slight increase of protein adsorption with the increase of the bilayers, while the membranes of M-SE showed an opposite result. The tendency of protein adsorption for the star-shaped polymer-deposited membranes could be explained by water contact angle, SEM, and AFM analyses. As mentioned above, materials possessing a hydrophilic surface normally showed lower protein adsorption, while the roughness of the material surface also had a large influence on protein adsorption. In this study, the M-SA membranes showed a slight increase of protein adsorption with the increase of the bilayers, which might be due to the increased rougher surfaces of the M-SA, while the increased roughness of the membrane surfaces of M-SE were much lower than that of the M-SA membrane surfaces according to the SEM and AFM images. Meanwhile, as widely known, the EGMA units had a more remarkable antiprotein adhesion ability than many other negatively charged polymers. Overall, the above protein adsorption results indicated that both the M-SA and the M-SE membranes revealed decreased plasma protein adsorption compared to the pristine membrane, which would benefit the improvement of blood compatibility.

3.4.2. Platelet Adhesion. For blood-contacting materials platelet adhesion is the key event during thrombus formation.[43] Many kinds of coagulation factors can be further activated by the activated platelets followed by acceleration of thrombosis and coagulations. In this study, platelet adhesion measurement was evaluated. As shown in Figure 4, both the spreading and formation of pseudopodium for the platelets were dramatically suppressed, indicating lowered platelet activation and improved blood compatibility by the star-shaped supramolecule-deposited heparin-mimicking 3D porous multilayer thin film surfaces.

Figure 4A-1, 4B-1, 4B-2, 4B-3, 4C-1, 4C-2, and 4C-3 shows SEM observation results of the platelets adhering onto the PES and star-shaped supramolecule-deposited membranes. It could be observed that on the pristine membrane surface a large number of platelets aggregated and accumulated. These platelets presented flattened and irregular shapes. However, on the star-shaped polymer-deposited membranes, few platelets were observed and the platelets adhering onto the modified membranes had a rounded morphology with almost no pseudopodium formation. Figure 4D shows the number of adherent platelets on the pristine and star-shaped polymer-deposited membranes. For the membranes M-SA-5, M-SA-15, and M-SA-25 the number of platelets decreased with the increase of the bilayers, which was consistent with the tendency

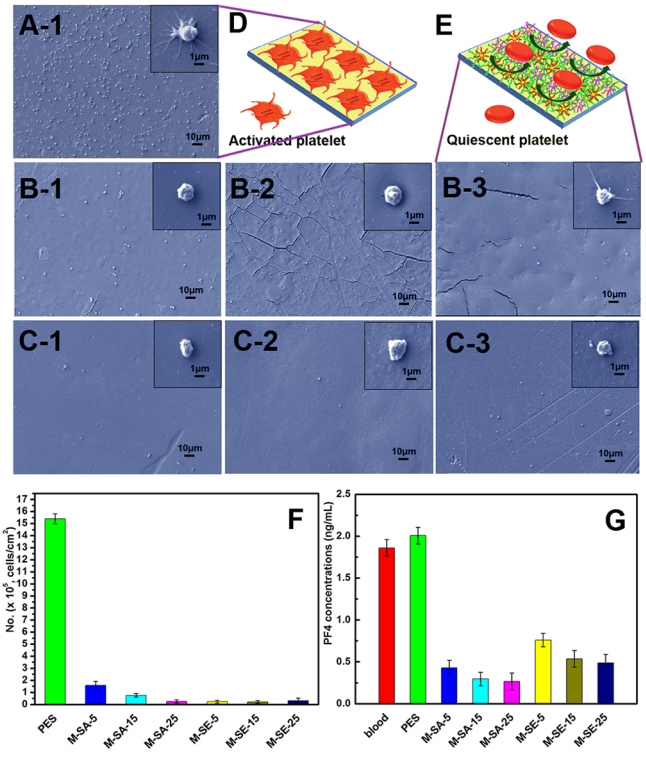

Figure 4. SEM images of platelets adhering to the PES (A-1), M-SA-5 (B-1), M-SA-15 (B-2), M-SA-25 (B-3), M-SE-5 (C-1), M-SE-15 (C-2), and M-SE-25 (C-3). Note, deformation of the surface morphology of the star-shaped polymer assembled layer resulted from the drying process due to immersion in organic solvents. (D) Activated platelets on PES membrane surface. (E) Antiplatelet adhesion and platelets remaining in quiescent after exposing with polymeric membrane. (F) Average numbers of the adhered platelets onto the membranes from PRP estimated via 7 SEM images. (G) Generated concentrations of PF4 of these samples with whole blood, which can act as an index for platelet activation; values are expressed as means ± SD, n = 3.

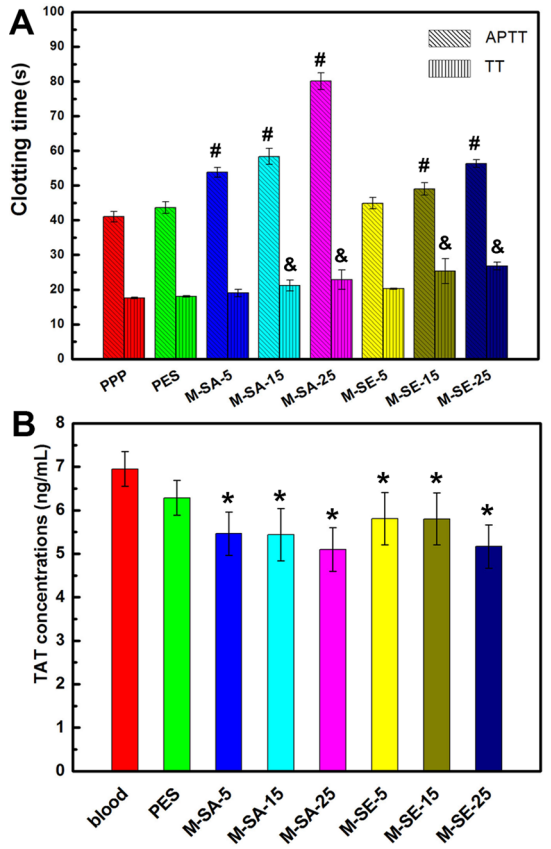

Figure 5. APTT and TT assays of the pristine membrane and star-shaped supramolecules assembled membranes; values were expressed as means ± SD, n = 3 (A), $^{\&}P$, $^{\#}P < 0.05$ compared to the value of PES. TAT generation of all membranes with blood flowing for 2 h; values were expressed as means ± SD, n = 3, $^{*}P < 0.05$ (B) compared to the value of PES.

of WCA results. For the M-SA-25, although some pseudopodium was observed, the platelet still kept a rounded morphology. For the membranes M-SE-5, M-SE-15, and M-SE-25, few platelets were observed and the platelets kept a rounded morphology with almost no pseudopodium formation; platelet adhesion onto the M-SE membranes was more fully suppressed compared to that for the M-SA membranes.

PF4 has been reported to play a vital role in inflammation and injury response.[44] Hence, PF4 was used to detect platelet activation by modified biomedical materials. Figure 4G shows the PF4 concentrations in plasma after the membrane surfaces contacted with blood; it could be observed that for the two series of membrane surfaces the PF4 concentration showed a prominent decrease compared with normal plasma or pristine PES membrane surface. Combined with the morphologies and numbers of the adhered platelets, these results indicated that platelet activation on the star-shaped supramolecule-deposited heparin-mimicking membrane surfaces did not occur or was greatly suppressed.[45]

3.4.3. Clotting Time (APTT and TT). Figure 5 shows the clotting times for the pristine, M-SA, and M-SE membranes. It could be observed that the APTTs for the modified membranes had a maximum increase by 39 s compared to the pristine membrane, while the TT increased with a maximum of 8.7 s. The results indicated that the modified biomedical membranes had an effect on the endogenous pathway of coagulation, which might be ascribed to the combination or reaction between the coagulation factors (V and X) in plasma and the hydrophilic surfaces of the modified biomedical membranes.

Thrombin generation was evaluated via detection of the TAT concentration, since the thrombin would be immediately neutralized by antithrombin III, resulting in TAT complex formation.[46] Figure 5B shows the TAT level in plasma after the membranes contact with blood, as observed from the TAT level in Figure 5B; the concentrations of TAT for the samples decreased compared to those of blood and pristine polymeric membrane. Furthermore, with the increase of the coated bilayers for the M-SA and M-SE membranes the generated TAT values decreased gradually. The results confirmed that the TAT generation was successfully suppressed by the star-shaped supramolecules-deposited heparin-mimicking multilayers; thus, combined with the platelet adhesion and activation results, it might be concluded that the surface-modified polymeric membranes showed excellent blood compatibility.

Meanwhile, Table S1, Supporting Information, shows a comparison of the anticoagulant activity among the star-shaped heparin-mimicking supramolecules, linear heparin-mimicking polymer, and heparin. The results indicated that heparin had the highest anticoagulant activity compared with star-shaped heparin-mimicking supramolecules and linear heparin-mimicking polymer, and the heparin-mimicking components could partially mimic the anticoagulant activity as heparin. Fur-

thermore, the star-shaped heparin-mimicking supramolecules showed higher anticoagulant activity than the linear heparin-like polymer at the same concentration. Thus, the anticoagulant data indicates that the hyperbranched structure can mimic heparin more effectively than the linear polymer, which may be due to the high density of the sulfonic acid and carboxyl acid groups and spatial conformation.

3.4.4. Blood-Related Complement Activation. Complement activation could be evaluated via determination of the generated anaphylatoxins C3a, C4a, and C5a. In this study, C3a and C5a were used to evaluate the complement activation using an ELISA assay.

Figure 6A and 6B shows the concentrations of C3a and C5a, respectively. It was found that the C3a concentrations for the

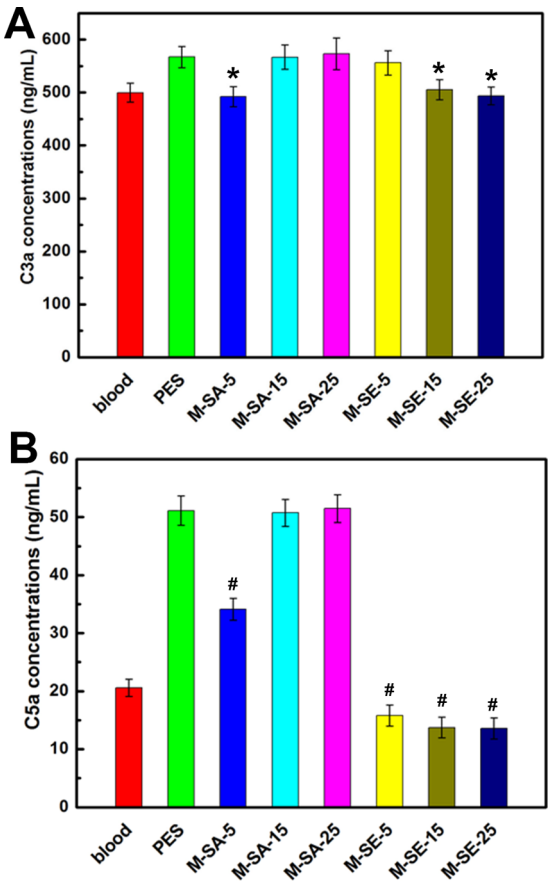

Figure 6. Concentrations of C3a for the membranes with whole blood (A); values are expressed as means ± SD, $n = 3$, $^{*}P < 0.05$ compared to the value of PES. Concentrations of C5a for the membranes with whole blood (B); values are expressed as means ± SD, $n = 3$, $^{\#}P < 0.05$ compared to the value of PES.

M-SA membrane surfaces increased slightly with the increase of the bilayers, which were finally higher than that for blood but commensurate with that for pristine membrane, while for the M-SE membrane surfaces it could be observed that the C3a concentrations decreased with the increase of the bilayers and finally commensurate with that for blood. The same changing tendency with the increase of the bilayers from 5 to 25 was obtained for C5a levels. The C5a concentrations for the M-SA were higher than that for blood but commensurate with that for pristine membrane. For the M-SE membrane surfaces, the C5a concentrations were lower than that for blood and pristine PES membrane. In general, the obtained results verified that the star-shaped supramolecule-deposited heparin-mimicking biomedical membranes exhibited lower blood-related complement activation than pristine membrane, which might have suppressed inflammation responses when contacted with blood.

3.5. Influence of Heparin-Mimicking Multilayer Modified Biomedical Membrane Surfaces on HUVECs Growth. HUVECs were cultured in vitro to measure the cytocompatibility of the star-shaped supramolecule-deposited biomedical membranes. It is known that the endothelial cell membrane is negatively charged and the cells communicate with the substratum through an adsorbed protein layer via proper specific recognition and binding sites formed between the adsorbed proteins and the cell membranes. Thus, the negatively charged surface might repulse the adsorption of protein from the culture medium and then block the anchorage of the negative HUVECs to the material surface.[47] However, the negatively charged heparin and heparin-mimicking polymer-modified surface is expected to be favorable for cell proliferation by immobilization of cellular fibronectin and thus exhibits extremely low cytotoxicity.[48,49] Thus, in this study, the star-shaped heparin-mimicking supramolecule-deposited biomedical membranes may also enhance the cell adhesion ability. HUVECs are selected as model cells to evaluate the cell viability of the modified biomedical membranes.

3.5.1. Cell Morphology. Morphologies of the HUVECs cultured for 6 days on the PES and star-shaped supramolecule-deposited membrane surfaces are shown in Figure 7. It was observed that the HUVECs exhibited a typical flattened morphology. As could be observed, few HUVECs were spread onto the surface of pristine PES membrane, while for the star-shaped heparin-mimicking supramolecule-deposited surfaces the HUVECs almost covered the whole surfaces, which spread with ruffling of peripheral cytoplasm. The results indicated that the star-shaped heparin-mimicking supramolecule-deposited surfaces could enhance cell adhesion and growth, since the HUVECs, which could express a high surface density of intercellular adhesion molecule, might be bound to the sulfonic group containing heparin-mimicking surfaces. Compared to the HUVECs adhered onto the M-SA and M-SE membranes, it was observed that the HUVECs on the M-SA were closed packing and the HUVECs on the M-SE were fully spread out. Thus, the surfaces of M-SA might be more suitable for growth of HUVECs.

Confocal microscopy techniques were carried out to further evaluate the morphologies of the cells seeded onto the surfaces of pristine PES and star-shaped supramolecule-deposited membranes. It was observed that the amount of the HUVECs on the pristine PES membrane was very low, and more HUVECs were adhered onto the surfaces of the M-SA compared with those of the M-SE (Figure 7). The HUVECs seeded onto the M-SA showed distinct regional aggregations compared to those for the M-SE, while for the M-SE the HUVECs displayed elongated morphology. The results confirmed that cell adhesion and growth was significantly promoted on the star-shaped supramolecule-deposited membrane surfaces.

3.5.2. MTT Assay. The cytotoxicity of the membranes was measured on HUVECs by MTT assay. The pristine PES membrane was used as control. Figure 8 shows the MTT results for the PES and modified biomedical membranes. Absorption of formazan indicated that the HUVECs were successfully seeded onto the PES and modified biomedical

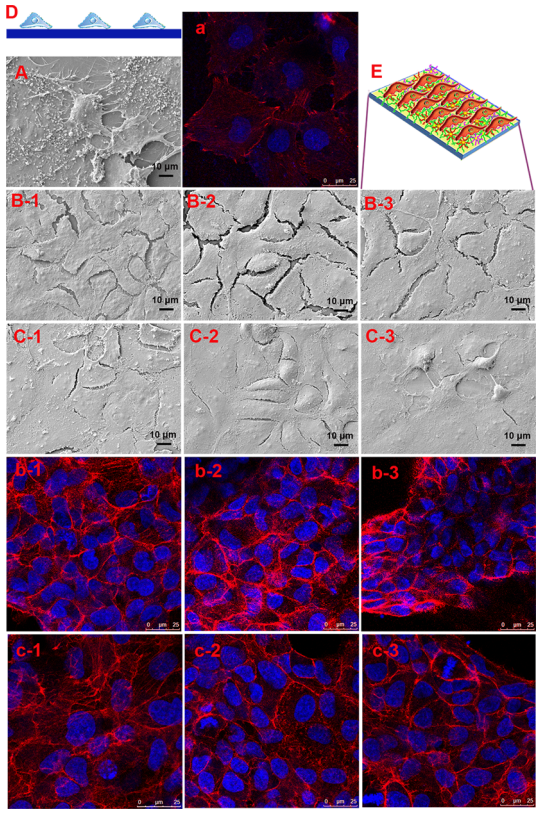

Figure 7. Morphologies of the HUVECs observed by SEM at a magnification of ×1000. The membranes: pristine polymeric membrane (A), M-SA-5 (B-1), M-SA-15 (B-2), M-SA-25 (B-3), M-SE-5 (C-1), M-SE-15 (C-2), M-SE-25 (C-3); images at a magnification of ×300 are shown in Figure S5, Supporting Information. Fluorescence staining images of the HUVECs cultured for 6 days on pristine and star-shaped supramolecule-deposited membranes. Pristine membrane (a), M-SA-5 (b-1), M-SA-15 (b-2), M-SA-25 (b-3), M-SE-5 (c-1), M-SE-15 (c-2), and M-SE-25 (c-3). (D and E) Cartoon images of the HUVECs adhesion on the pristine membrane and star-shaped supramolecule-deposited membranes, respectively.

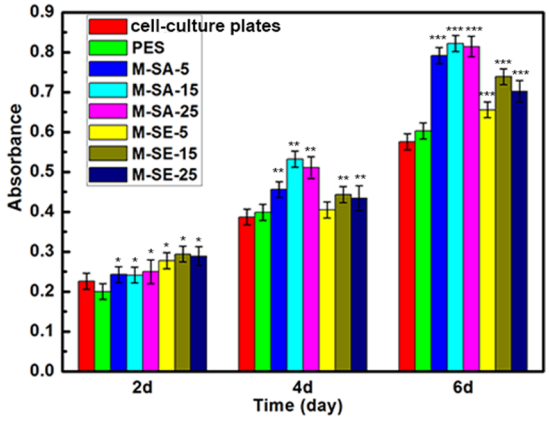

Figure 8. MTT tetrazolium assays. Formazan absorbance is expressed as a function of time for the HUVECs seeded onto different membranes and the control; values are expressed as mean ± SD of eight determinations. *P, **P, ***P < 0.05 compared to the values for the PES membranes at 2, 4, and 6 days, respectively.

membranes. As shown in Figure 8, on the second, fourth, and sixth days the viability of the cells on the heparin-mimicking biomedical membranes increased compared with the PES. It was observed that the M-SA-15 and M-SE-15 membranes exhibited the best cytocompatibility among the M-SA membranes and M-SE membranes, respectively. It is known that the cell−material surface interaction is influenced by various factors such as surface charge, surface wettability, free energy, surface morphology, roughness, the existence of bioactive factors, etc. Thus, the changing tendency of MTT data for these samples might be influenced by these complicated factors. In general, it could be concluded that compared to the pristine PES membrane the star-shaped supramolecule-deposited multilayer thin film surfaces would show lower cytotoxicity and better cell viability. Thus, the heparin-mimicking biomedical membranes should have great potential in applications of the biological and biomedical fields.

4. CONCLUSIONS

In this study, surface LbL-assembled 3D porous multilayers were constructed on polymeric membranes using the star-shaped supramolecules. Surface ATR-FTIR spectra, XPS data, SEM, and AFM images confirmed successful deposition of the star-shaped polymers onto the membrane surfaces, and the as-prepared surface-coated PES membranes exhibited 3D porous surface morphologies. Meanwhile, the coating surface of PVDF and PSf membranes also exhibited 3D porous morphologies as PES membrane surface, which indicated that this proposed strategy could also be applied in the surface coating of many other polymeric membrane substrates. In the systematic in vitro blood compatibility tests the modified PES membranes performed decreased water contact angle, declined protein adsorption, prolonged clotting time, and suppressed platelet adhesion compared to pristine PES membrane, which indicated the heparin-mimicking multilayers-coated membranes showed ultralow blood components activation and excellent hemocompatibility. The cytocompatibility experiment further indicated that the star-shaped supramolecule-deposited 3D porous multilayers had a positive effect on endothelial cell attachment and growth. Thus, the star-shaped supramolecule-deposited 3D porous heparin-mimicking multilayer thin films might have promising application in the surface modification of polymeric membranes and also some other blood-contacting biomedical fields.

■ ASSOCIATED CONTENT

Ⓢ Supporting Information

FTIR spectra of the star-shaped supramolecules; surface SEM images for pristine PVDF and PSf membranes, and the surface SEM images of corresponding SA and SE coated 15 bilayers; ATR-FTIR and XPS spectra of M-SA and M-SE; cross-section SEM images for M-SA-15 and M-SE-15; SEM images for the morphologies of HUVECs at a magnification of ×300; Quantification of the numbers of the adherent cells. This material is available free of charge via the Internet at http://pubs.acs.org.

■ AUTHOR INFORMATION

Corresponding Authors

*E-mail: sagecheng@163.com or chengcho@umich.edu.
*E-mail: zhaochsh70@163.com or zhaochsh70@scu.edu.cn.

Notes

The authors declare no competing financial interest.

■ ACKNOWLEDGMENTS

Xinyue Liu and Lang Ma contributed equally to this work. This work was financially sponsored by the National Natural Science Foundation of China (Nos. 51225303 and 51433007). We also thank our laboratory members for their generous help and gratefully acknowledge the help of Ms. H. Wang of the Analytical and Testing Center at Sichuan University for SEM.

■ REFERENCES

(1) Place, E. S.; George, J. H.; Williams, C. K.; Stevens, M. M. Synthetic Polymer Scaffolds for Tissue Engineering. *Chem. Soc. Rev.* **2009**, *38*, 1139−1151.

(2) Elam, J.-H.; Nygren, H. Adsorption of Coagulation Proteins from Whole Blood on to Polymer Materials: Relation to Platelet Activation. *Biomaterials* **1992**, *13*, 3−8.

(3) Ran, F.; Nie, S.; Li, J.; Su, B.; Sun, S.; Zhao, C. Heparin-Like Macromolecules for the Modification of Anticoagulant Biomaterials. *Macromol. Biosci.* **2012**, *12*, 116−125.

(4) Francois, P.; Vaudaux, P.; Nurdin, N.; Mathieu, H.; Descouts, P.; Lew, D. P. Physical and Biological Effects of a Surface Coating Procedure on Polyurethane Catheters. *Biomaterials* **1996**, *17*, 667−678.

(5) Tang, M.; Xue, J.; Yan, K.; Xiang, T.; Sun, S.; Zhao, C. Heparin-Like Surface Modification of Polyethersulfone Membrane and Its Biocompatibility. *J. Colloid Interface Sci.* **2012**, *386*, 428−440.

(6) Mader, J. S.; Smyth, D.; Marshall, J.; Hoskin, D. W. Bovine Lactoferricin Inhibits Basic Fibroblast Growth Factor- and Vascular Endothelial Growth Factor (165)-Induced Angiogenesis by Competing for Heparin-Like Binding Sites on Endothelial Cells. *Am. J. Pathol.* **2006**, *169*, 1753−1766.

(7) Poetschke, C.; Selleng, S.; Broeker, B. M.; Greinacher, A. Heparin-Induced Thrombocytopenia: Further Evidence for a Unique Immune Response. *Blood* **2012**, *120*, 4238−4245.

(8) Uchman, M.; Stepanek, M.; Prochazka, K.; Mountrichas, G.; Pispas, S.; Voets, I. K.; Walther, A. Multicompartment Nanoparticles Formed by a Heparin-Mimicking Block Terpolymer in Aqueous Solutions. *Macromolecules* **2009**, *42*, 5605−5613.

(9) Christman, K. L.; Vazquez-Dorbatt, V.; Schopf, E.; Kolodziej, C. M.; Li, R. C.; Broyer, R. M.; Chen, Y.; Maynard, H. D. Nanoscale Growth Factor Patterns by Immobilization on a Heparin-Mimicking Polymer. *J. Am. Chem. Soc.* **2008**, *130*, 16585−16591.

(10) Balani, K.; Anderson, R.; Laha, T.; Andara, M.; Tercero, J.; Crumpler, E.; Agarwal, A. Plasma-Sprayed Carbon Nanotube Reinforced Hydroxyapatite Coatings and Their Interaction with Human Osteoblasts in Vitro. *Biomaterials* **2007**, *28*, 618−624.

(11) Ma, L.; Qin, H.; Cheng, C.; Xia, Y.; He, C.; Nie, C.; Wang, L.; Zhao, C. Mussel-Inspired Self-Coating at Macro-Interface with Improved Biocompatibility and Bioactivity Via Dopamine Grafted Heparin-Like Polymers and Heparin. *J. Mater. Chem. B* **2014**, *2*, 363−375.

(12) Sharkawi, T.; Darcos, V.; Vert, M. Poly(Dl-Lactic Acid) Film Surface Modification with Heparin for Improving Hemocompatibility of Blood-Contacting Bioresorbable Devices. *J. Biomed. Mater. Res., Part A* **2011**, *98A*, 80−87.

(13) Perrenoud, I. A.; Rangel, E. C.; Mota, R. P.; Durrant, S. F.; da Cruz, N. C. Evaluation of Blood Compatibility of Plasma Deposited Heparin-Like Films and Sf6 Plasma Treated Surfaces. *Mater. Res.* **2010**, *13*, 95−98.

(14) Zhou, H.; Cheng, C.; Qin, H.; Ma, L.; He, C.; Nie, S.; Zhang, X.; Fu, Q.; Zhao, C. Self-Assembled 3d Biocompatible and Bioactive Layer at the Macro-Interface Via Graphene-Based Supermolecules. *Polym. Chem.* **2014**, *5*, 3563−3575.

(15) Ran, F.; Niu, X.; Song, H.; Cheng, C.; Zhao, W.; Nie, S.; Wang, L.; Yang, A.; Sun, S.; Zhao, C. Toward a Highly Hemocompatible Membrane for Blood Purification Via a Physical Blend of Miscible Comb-Like Amphiphilic Copolymers. *Biomater. Sci.* **2014**, *2*, 538−547.

(16) Ma, L.; Su, B.; Cheng, C.; Yin, Z.; Qin, H.; Zhao, J.; Sun, S.; Zhao, C. Toward Highly Blood Compatible Hemodialysis Membranes Via Blending with Heparin-Mimicking Polyurethane: Study in Vitro and in Vivo. *J. Membr. Sci.* **2014**, *470*, 90−101.

(17) Ariga, K.; Lvov, Y. M.; Kawakami, K.; Ji, Q.; Hill, J. P. Layer-by-Layer Self-Assembled Shells for Drug Delivery. *Adv. Drug Delivery Rev.* **2011**, *63*, 762−771.

(18) Chen, Y.; Zeng, G.; Pan, F.; Wang, J.; Chi, L. Controlled Assembly and Release of Retinoic Acid Based on the Layer-by-Layer Method. *Langmuir* **2013**, *29*, 2708−2712.

(19) Mansouri, S.; Merhi, Y.; Winnik, F. M.; Tabrizian, M. Investigation of Layer-by-Layer Assembly of Polyelectrolytes on Fully Functional Human Red Blood Cells in Suspension for Attenuated Immune Response. *Biomacromolecules* **2011**, *12*, 585−592.

(20) Boddohi, S.; Killingsworth, C. E.; Kipper, M. J. Polyelectrolyte Multilayer Assembly as a Function of Ph and Ionic Strength Using the Polysaccharides Chitosan and Heparin. *Biomacromolecules* **2008**, *9*, 2021−2028.

(21) Ma, R. Z.; Sasaki, T.; Bando, Y. Layer-by-Layer Assembled Multilayer Films of Titanate Nanotubes, Ag- or Au-Loaded Nanotubes, and Nanotubes/Nanosheets with Polycations. *J. Am. Chem. Soc.* **2004**, *126*, 10382−10388.

(22) Shutava, T. G.; Balkundi, S. S.; Vangala, P.; Steffan, J. J.; Bigelow, R. L.; Cardelli, J. A.; O'Neal, D. P.; Lvov, Y. M. Layer-by-Layer-Coated Gelatin Nanoparticles as a Vehicle for Delivery of Natural Polyphenols. *ACS Nano* **2009**, *3*, 1877−1885.

(23) Balani, K.; Chen, Y.; Harlinkar, S. P.; Dahotre, N. B.; Agarwal, A. Tribological Behavior of Plasma-Sprayed Carbon Nanotube-Reinforced Hydroxyapatite Coating in Physiological Solution. *Acta Biomater.* **2007**, *3*, 944−951.

(24) Gou, P.-F.; Zhu, W.-P.; Shen, Z.-Q. Synthesis, Self-Assembly, and Drug-Loading Capacity of Well-Defined Cyclodextrin-Centered Drug-Conjugated Amphiphilic a(14)B(7) Miktoarm Star Copolymers Based on Poly(Epsilon-Caprolactone) and Poly(Ethylene Glycol). *Biomacromolecules* **2010**, *11*, 934−943.

(25) Hu, Y.; Zhu, Y.; Yang, W. T.; Xu, F. J. New Star-Shaped Carriers Composed of Beta-Cyclodextrin Cores and Disulfide-Linked Poly-(Glycidyl Methacrylate) Derivative Arms with Plentiful Flanking Secondary Amine and Hydroxyl Groups for Highly Efficient Gene Delivery. *ACS Appl. Mater. Interfaces* **2013**, *5*, 703−712.

(26) Li, J. S.; Xiao, H. N.; Kim, Y. S.; Lowe, T. L. Synthesis of Water-Soluble Cationic Polymers with Star-Like Structure Based on Cyclodextrin Core Via Atrp. *J. Polym. Sci., Part A: Polym. Chem.* **2005**, *43*, 6345−6354.

(27) Xu, F. J.; Zhang, Z. X.; Ping, Y.; Li, J.; Kang, E. T.; Neoh, K. G. Star-Shaped Cationic Polymers by Atom Transfer Radical Polymerization from Beta-Cyclodextrin Cores for Nonviral Gene Delivery. *Biomacromolecules* **2009**, *10*, 285−293.

(28) Wu, Y.; Ni, P.; Zhang, M.; Zhu, X. Fabrication of Microgels Via Supramolecular Assembly of Cyclodextrin-Containing Star Polycations and Oppositely Charged Linear Polyanions. *Soft Matter* **2010**, *6*, 3751−3758.

(29) Hay, R. W.; Lawrance, G. A.; Curtis, N. F. A Convenient Synthesis of the Tetra-Aza-Macrocyclic Ligands Trans-[14]-Diene, Tet a, and Tet B. *J. Chem. Soc., Perkin Trans. 1* **1975**, 591−593.

(30) Li, J. S.; Xiao, H. N. An Efficient Synthetic-Route to Prepare 2,3,6-Tri-O-(2-Bromo-2-Methylpropionyl -Beta-Cyclodextrin). *Tetrahedron Lett.* **2005**, *46*, 2227−2229.

(31) Mauricio, M. R.; Otsuka, I.; Borsali, R.; Petzhold, C. L.; Cellet, T. S. P.; de Carvalho, G. M.; Rubira, A. F. Synthesis of Star Poly(N-Isopropylacrylamide) by Beta-Cyclodextrin Core Initiator Via Atrp Approach in Water. *React. Funct. Polym.* **2011**, *71*, 1160−1165.

(32) Cheng, C.; Li, S.; Zhao, W.; Wei, Q.; Nie, S.; Sun, S.; Zhao, C. The Hydrodynamic Permeability and Surface Property of Polyethersulfone Ultrafiltration Membranes with Mussel-Inspired Polydopamine Coatings. *J. Membr. Sci.* **2012**, *417*, 228−236.

(33) Cai, K. Y.; Rechtenbach, A.; Hao, J. Y.; Bossert, J.; Jandt, K. D. Polysaccharide-Protein Surface Modification of Titanium Via a Layer-by-Layer Technique: Characterization and Cell Behaviour Aspects. *Biomaterials* **2005**, *26*, 5960−5971.

(34) Shen, J.; Hu, Y.; Li, C.; Qin, C.; Shi, M.; Ye, M. Layer-by-Layer Self-Assembly of Graphene Nanoplatelets. *Langmuir* **2009**, *25*, 6122−6128.
(35) Cheng, C.; Li, S.; Nie, S.; Zhao, W.; Yang, H.; Sun, S.; Zhao, C. General and Biomimetic Approach to Biopolymer-Functionalized Graphene Oxide Nanosheet through Adhesive Dopamine. *Biomacromolecules* **2012**, *13*, 4236−4246.
(36) Jee, K. S.; Dal Park, H.; Park, K. D.; Ha Kim, Y.; Shin, J. W. Heparin Conjugated Polylactide as a Blood Compatible Material. *Biomacromolecules* **2004**, *5*, 1877−1881.
(37) Xia, Y.; Cheng, C.; Wang, R.; Qin, H.; Zhang, Y.; Ma, L.; Tan, H.; Gu, Z.; Zhao, C. Surface-Engineered Nanogel Assemblies with Integrated Blood Compatibility, Cell Proliferation and Antibacterial Property: Towards Multifunctional Biomedical Membranes. *Polym. Chem.* **2014**, *5*, 5906−5919.
(38) Cheng, C.; Nie, S.; Li, S.; Peng, H.; Yang, H.; Ma, L.; Sun, S.; Zhao, C. Biopolymer Functionalized Reduced Graphene Oxide with Enhanced Biocompatibility Via Mussel Inspired Coatings/Anchors. *J. Mater. Chem. B* **2013**, *1*, 265−275.
(39) Medzhitov, R. Recognition of Microorganisms and Activation of the Immune Response. *Nature* **2007**, *449*, 819−826.
(40) Chen, J.; Guo, J.; Chang, B.; Yang, W. Blue-Emitting Pegylated Hyperbranched Pamam: Transformation of Cross-Linked Micelles to Hollow Spheres Controlled by the Peg Grafting Density. *Colloid Polym. Sci.* **2012**, *290*, 517−524.
(41) Ishihara, K.; Fukumoto, K.; Iwasaki, Y.; Nakabayashi, N. Modification of Polysulfone with Phospholipid Polymer for Improvement of the Blood Compatibility. Part 2. Protein Adsorption and Platelet Adhesion. *Biomaterials* **1999**, *20*, 1553−1559.
(42) Herrwerth, S.; Eck, W.; Reinhardt, S.; Grunze, M. Factors That Determine the Protein Resistance of Oligoether Self-Assembled Monolayers - Internal Hydrophilicity, Terminal Hydrophilicity, and Lateral Packing Density. *J. Am. Chem. Soc.* **2003**, *125*, 9359−9366.
(43) Gorbet, M. B.; Sefton, M. V. Biomaterial-Associated Thrombosis: Roles of Coagulation Factors, Complement, Platelets and Leukocytes. *Biomaterials* **2004**, *25*, 5681−5703.
(44) Niewiarowski, S.; Thomas, D. P. Platelet Factor 4 and Adenosine Diphosphate Release During Human Platelet Aggregation. *Nature* **1969**, *222*, 1269−70.
(45) Nie, S.; Qin, H.; Cheng, C.; Zhao, W.; Sun, S.; Su, B.; Zhao, C.; Gu, Z. Blood Activation and Compatibility on Single-Molecular-Layer Biointerfaces. *J. Mater. Chem. B* **2014**, *2*, 4911−4921.
(46) Nie, S.; Tang, M.; Cheng, C.; Yin, Z.; Wang, L.; Sun, S.; Zhao, C. Biologically Inspired Membrane Design with a Heparin-Like Interface: Prolonged Blood Coagulation, Inhibited Complement Activation, and Bio-Artificial Liver Related Cell Proliferation. *Biomater. Sci.* **2014**, *2*, 98−109.
(47) Zhu, Y. B.; Sun, Y. The Influence of Polyelectrolyte Charges of Polyurethane Membrane Surface on the Growth of Human Endothelial Cells. *Colloids Surf., B* **2004**, *36*, 49−55.
(48) Mammadov, R.; Mammadov, B.; Toksoz, S.; Aydin, B.; Yagci, R.; Tekinay, A. B.; Guler, M. O. Heparin Mimetic Peptide Nanofibers Promote Angiogenesis. *Biomacromolecules* **2011**, *12*, 3508−3519.
(49) Whitelock, J. M.; Iozzo, R. V. Heparan Sulfate: A Complex Polymer Charged with Biological Activity. *Chem. Rev.* **2005**, *105*, 2745−2764.